



Magnetic and Magnetotransport Properties of Memory Sensors Based on Anisotropic Magnetoresistance

E. Demirci¹

Received: 14 July 2020 / Accepted: 10 August 2020 / Published online: 20 August 2020
© Springer Science+Business Media, LLC, part of Springer Nature 2020

Abstract

The magnetic and magnetoresistance properties of anisotropic magnetoresistance (AMR) sensors based on Wheatstone bridge (WB) with barber pole and conventional Hall bar structures were studied. The samples were prepared by using standard microlithography and sputter deposition techniques and then measured by magneto-optic Kerr effect and magneto transport methods. The advantages of the AMR sensor based on WB compared with Hall bar structure were discussed. It was observed that sensitivity was increased almost 15 times when sensors with the WB structures were used instead of Hall bar structures. Moreover, sensor stability was tested in various external magnetic fields with positive and negative polarities. The test results show that sensor response is stable even in various external magnetic fields up to 5000 Oe. The changes in sensitivity and output voltage were attributed to WB structure.

Keywords Anisotropic magnetoresistance (AMR) · Wheatstone bridge · barber pole · electrical output voltage · sensor sensitivity

1 Introduction

In recent years, several types of magnetic sensors were used in practical applications such as giant magnetoresistance [1, 2], giant magnetoimpedance [3, 4], tunneling magnetoresistance/spin-dependent tunneling [5], and Hall effect [6]. Although they have a wide range of practical applications, many of these sensors generally work at relatively high magnetic fields and offer increased volume and power consumption. To overcome these critical disadvantages, the sensors based on anisotropic magnetoresistance (AMR) are mostly preferred due to their high sensitivity, the flexibility of the design, and compatibility with standard microelectronics technology. But the AMR sensors need to combine logic and memory on a single integrated circuit, and this case would require high sensitivity. The barber pole structures are a perfect design for such an application. The barber pole structures are highly sensitive at weak magnetic fields, and the energy consumption of these structures is very low for magnetic field sensors [7–10]. Another substantial advantage of the AMR sensors with barber pole structure

is that they give rise to linear electrical output voltage under the various external magnetic field (H_{ext}). Undoubtedly, this situation will significantly increase the interest in AMR sensors with barber pole structure due to their practical applications in navigation applications [11], flexible spintronic devices [12, 13], and space science [14].

It is known that the AMR effect arises from the anisotropic scattering of conductive electrons with uncompensated spins, and it strongly depends on the angle (θ) between the magnetization (M) and the current density (J) [15–17]. Since the direction of current density is parallel to the long axis of the Hall bar structure, the magnetization direction can be rotated by the H_{ext} for the conventional Hall bar structures. Unlike the conventional Hall bar structures, the direction of current density through the sample can be rotated by an angle of 45° or 135° due to the design of barber pole structures in the absence of a H_{ext} [18]. Moreover, AMR sensors are very sensitive to temperature changes and resistance fluctuation noise [19, 20]. In particular, the temperature effect on the resistivity of the sensor is a major problem. To avoid these negative effects, sensors based on the AMR effect are generally designed in the form of Wheatstone bridge structures. Wheatstone bridge structures typically consist of two parallel branches containing four resistors, and each of the four branches of a Wheatstone bridge is an AMR sensor. Since AMR cells show opposite resistance, the total resistance of four branches is stable even

✉ E. Demirci
e.demirci@gtu.edu.tr

¹ Department of Physics, Gebze Technical University,
41400 Kocaeli, Turkey

under the H_{ext} . Therefore, the total response in the Wheatstone bridge design is four times greater than a single sensor structure. Besides, another advantage of the Wheatstone bridge structure is that it can convert very small changes in resistance to a measurable electrical voltage.

In this study, the AMR sensor consisting of a Wheatstone bridge structure with barber pole design (WB) was compared with the Hall bar structure with respect to the electrical and magnetic properties. In the studied sample structures, magnetoresistive permalloy (Py: $\text{Ni}_{80}\text{Fe}_{20}$) was preferred as a ferromagnetic layer because it shows a high anisotropy ratio, low anisotropy and low ripple, long-term stability, and close to zero magnetostriction constant [21]. Also, gold (Au) was chosen as shorting bars top of the Py layer owing to its low resistivity material. It was also considered that Au thickness is large enough to eliminate the shunting effect [22]. Unlike the similar studies [10, 13], the thickness of the Au shorting bars top of the Py layer is very thin (30 nm) and the distance between two barber poles is 2 μm in this study. This provides a great advantage in spintronic device applications since the current direction passing through the Py layer is much more stable.

2 Sample Preparation

The reference sample with Hall bar structure (Py/Pt) and AMR sensor with a WB (Py/Pt/Cu/Au) were prepared by using microlithography and magnetron-sputter deposition techniques. First, patterning of WB and Hall bar structures was realized on SiO_2/Si substrates through the instrument of SUSS MicroTec MJB4 mask aligner. Then, magnetoresistive Py/Pt layers were grown on patterned SiO_2/Si substrate by magnetron sputtering of Pt (DC 10 W) and Py (RF 20 W) targets. The base pressure of the sputter chamber was kept 6×10^{-9} mbar before the deposition, and the sputtering pressure was kept at 5×10^{-3} mbar during the deposition. All growth processes were performed at room temperature. The in-plane aspect ratio of Py (10 nm)/Pt (5 nm) with the rectangular bar-shape was kept 30:1. In this way, the magnetization of the sensors was induced by shape anisotropy and it was directed along the long axis of Hall bar structure. Shorting bars on the barber pole structures and contact terminals were grown by the thermal evaporator. The thickness of Au shorting bars is 30 nm, and the thickness of the Cr layer used as a buffer layer between Au and Py is 5 nm. Figure 1a shows the photograph of the $\text{Si}/\text{SiO}_2/\text{Py}$ (10 nm)/Pt (5 nm) reference sample mounted on a printed circuit board. The reference sample consists of two regions. The upper side of the sample is the Hall bar structures, and the lower side of the sample is the continuous film as shown in Fig. 1a. Figure 1b presents the microscope top view image of the $\text{Si}/\text{SiO}_2/\text{Py}$ (10 nm)/Pt (5 nm)/Cr (5 nm)/Au (30 nm) AMR sensor with a WB.

Here, there are four individual AMR cells and the magnetic resistance of each cell is transformed into a voltage output due to the Wheatstone bridge structure. Furthermore, J through the Py layer is rotated by an θ angle of 45° or 135° thanks to barber pole design. Thus, the total resistance of the cells is kept steady and the temperature changes and resistance fluctuations are reduced.

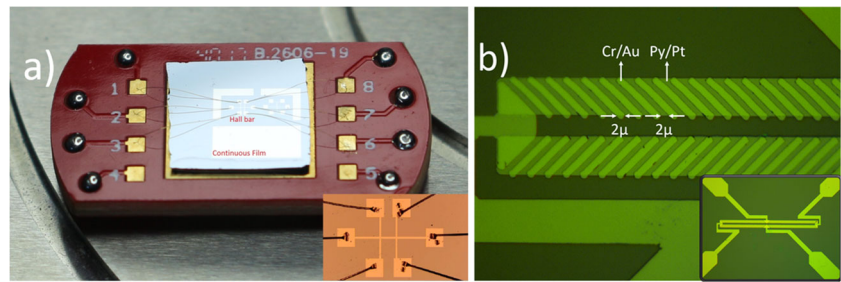
In this study, the magneto-optical Kerr effect (MOKE) system was used for magnetization experiments of the samples at room temperature. In addition, for the angle-dependent magnetization measurements from 0 to 360° , a stepper motor at longitudinal MOKE geometry was used. Magnetoresistive experiments were carried out by using a magnetotransport measurement system. A typical current strength was supplied by a source meter (Keithley 2400), and the current was fixed at 50 μA for all magnetoresistive experiments. The magnetic field-dependent output voltage was recorded by a nanovoltmeter (Keithley 2182).

3 Experiments and Discussion

Magnetic characterizations of the reference sample of $\text{Si}/\text{SiO}_2/\text{Py}$ (10 nm)/Pt (5 nm) were performed at in-plane geometry from 0 to 360° by using L-MOKE technique. Then, the normalized remanent magnetization (M_R/M_S) as a function of the angle was extracted from the magnetization curves measured for the reference sample as shown in Fig. 2a. The reference sample has the in-plane uniaxial magnetic anisotropy as obviously seen in the figure. This type of anisotropy is usually observed in polycrystalline samples and it is called growth induced anisotropy [23]. Figure 2b shows the hysteresis curves of the reference sample measured at the angles of 0° and 90° . A typical easy axis and the hard axis curves were observed at $\varphi = 0^\circ$ (solid circles) and $\varphi = 90^\circ$ (open circles), respectively. The easy axis of magnetization prefers to extend along the Hall bar of the reference sample due to the growth-induced magnetic anisotropy. In this way, M and J will be parallel to the easy axis and occurs the highest probability of scattering for the magnetoresistive experiments.

In this study, two types of magnetoresistive experiments were carried out of the reference sample in order to determine the relationship between the resistance (R) and H_{ext} . First, the angle-dependent behavior of the AMR voltage between 0 and 360° was measured while the H_{ext} value was constant. Figure 3a shows the angle-dependent AMR ratio for reference sample under 500 Oe magnetic field. Here, the AMR ratio is maximum in case of the M and J are parallel at $\varphi = 0^\circ$ (R_{\parallel}) and the AMR ratio is minimum in case of the M and J are perpendicular at $\varphi = 90^\circ$ (R_{\perp}). In addition, the angle-dependent AMR ratio of the reference sample shown in Fig. 2a is compatible with the angle-dependent behavior of the normalized M_R/M_S values obtained by the L-MOKE method shown in Fig. 3a.

Fig. 1 **a** Photograph of the reference sample with the Hall bar structure. **b** Enlarged microscope top view image of the Cr/Au strips with a width of $2\ \mu$ on Py/Pt layer. The image at the inset (**b**) shows Si/SiO₂/Py (10 nm)/Pt (5 nm)/Cr (5 nm)/Au (30 nm) structure that consists of four AMR sensors



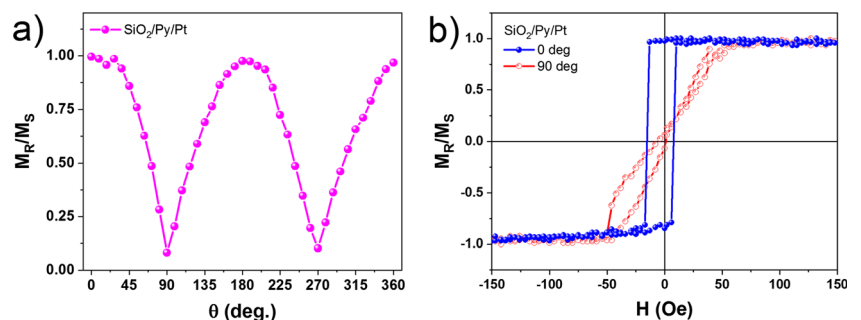
The second type of measurement method was the magnetic field–dependent behavior of AMR voltage at a fixed angle. These type measurements were carried out in the range of ± 300 Oe while the H_{ext} was fixed at 0° and 90° , respectively. First of all, the position of the reference sample was kept at 0° in order to bring M parallel to J and then the AMR voltage of reference sample was measured. After that, the AMR ratio was calculated by AMR ratio formula as shown in Fig. 3b. The AMR ratio is equal to $(R_{//} - R_{\perp}) / R_{\perp}$. The reference sample exhibited a 0.2% AMR ratio as obviously seen in the figure. After that, the reference sample was rotated 90° and M became perpendicular to J . At this angle, the reference sample exhibited a 0.03% AMR ratio as shown in Fig. 3c.

It is quite obvious that the reference sample had a low AMR ratio. Here, the WB was preferred instead of the Hall bar structure to increase the low AMR ratio. AMR sensor based on WB structure consists of Si/SiO₂/Py (10 nm)/Pt (5 nm)/Cr (5 nm)/Au (20 nm). Two types of magnetoresistive experiments were also performed for the WB structure. First, the angle-dependent electrical output (U) of the Wheatstone bridge was performed while the H_{ext} value was constant as given in Fig. 4a. During the measurements, an external in-plane magnetic field was 500 Oe of constant magnitude. When the M and J are parallel at $\varphi = 0^\circ$, U has the minimum value, contrarily when M and J are perpendicular $\varphi = 90^\circ$, U has maximum. In addition to this, the calculated electrical output ratio is 3.7% for the AMR sensor based on the WB structure. The sensor was also exhibited uniaxial magnetic anisotropy like the reference sample. However, the periodically anisotropic behavior of the AMR sensor based on the WB structure in Fig. 4a shifted 90° from the anisotropic behavior of the reference sample in Fig. 3a. This relates to whether the

applied H_{ext} and J are parallel or anti-parallel to each other [15, 24]. Secondly, magnetic field–dependent AMR voltage of the sensor based on WB structure was measured at a fixed angle. Figure 4b shows the AMR ratio for sensor based on WB structure while M and J were parallel. During this measurement, the direction of H_{ext} was settled at 0° , and the magnitude of H_{ext} was changed between $+200$ and -200 Oe. The AMR ratio was determined as 0.6% for the sensor based on the WB structure. Then, the AMR sensor based on WB structure was rotated 90° and M was become perpendicular to J . At this angle, the sensor structure exhibited a 1% AMR ratio as shown in Fig. 4c. The AMR ratios for both samples were compared, and the results showed that the AMR ratio and output voltage were significantly increased due to the WB design.

Furthermore, H_{ext} at the different magnitudes was applied to the AMR sensor based on WB structure to affirm the angular dependence of AMR on both the field orientations and magnitude. The angle-dependent electrical output was measured under the constant magnetic field and at the angles between 0 and 360° in steps of 10° as shown in Fig. 5a. After each measurement, the magnitude of the constant magnetic field was gradually increased from 20 to 5000 Oe and the angle-dependent electrical output measurements were repeated under the constant field depending on the direction angle of the H_{ext} . In the range of 50 Oe and 5000 Oe which is higher than the saturation field of the AMR sensor based on WB structure, the U - θ curve matched very well with an electrical field (E) for a single domain FM metal film in the Eq. (1). For $H = 20$ Oe; however, it was observed that there was a difference from the theoretically predicted behavior. The reason for this unusual behavior in the U is that the H_{ext} is not sufficient

Fig. 2 Magnetic characterization of the reference sample. **a** Angle-dependent behavior of the normalized remanent magnetization (M_R/M_S) values obtained by the L-MOKE method. **b** Magnetization curves of the sample taken at the angles of 0° (solid circles) and 90° (open circles)



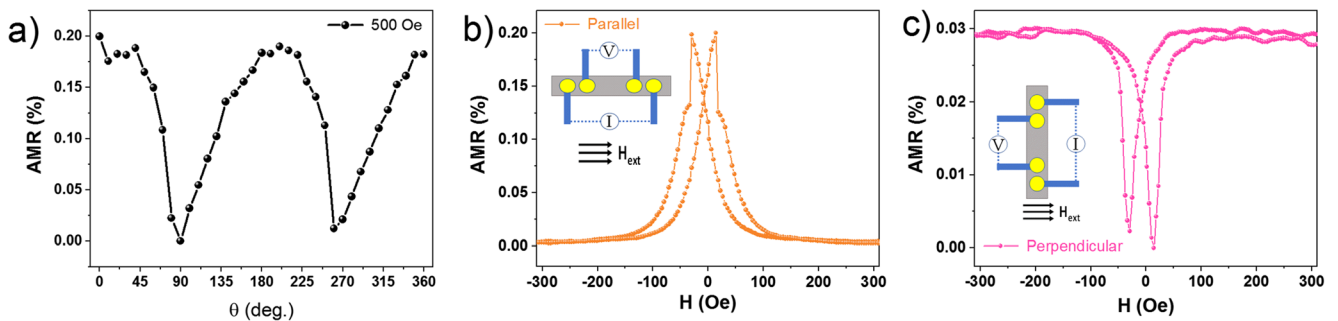


Fig. 3 Magnetoresistance characterizations of the reference sample. **a** Angle-dependent AMR ratio of reference sample under a magnetic field of 500 Oe. **b** AMR ratio of reference sample when M and J are parallel. **c** AMR ratio of reference sample when M and J are perpendicular

to reach saturation of the Py magnetic moments in the AMR sensor based on WB structure.

$$E = j\rho_{\perp} + j\left(\rho_{\parallel} - \rho_{\perp}\right)\cos^2\theta \quad (1)$$

where ρ_{\parallel} and ρ_{\perp} refer to resistivities for current parallel and perpendicular to the magnetic field, respectively. θ is the angle between the M and the J .

For the low external magnetic fields, the effect of magnetocrystal anisotropy can explain this difference in the angular dependence of AMR [25, 26]. The Py magnetic moments in the AMR sensor based on WB structure in the case of the H_{ext} at lower than the saturation field of the sensor cannot stay in a single domain. Thus, the magnetocrystal anisotropy became dominant against the external magnetic field and the U - θ curve did not match very well with an electrical field for the 20 Oe constant magnetic field. On the other hand, H_{ext} that is higher than the saturation field overcomes the magnetocrystalline anisotropy and magnetic moments of the sample align along the H_{ext} [27].

Various H_{ext} with positive and negative polarities was applied to the sensor. The magnitude of the H_{ext} was fixed and applied to the sensor in different polarities every 50 s in order to detect the stability of the AMR sensor based on WB structure. The sensor output voltage was recorded under 0 Oe, H_{positive} , 0 Oe, and H_{negative} magnetic fields, respectively as shown in Fig. 5b. This process was repeated 5 times consecutively. The

magnitude of the H_{ext} was then gradually increased from 20 to 5000 Oe, and the electrical output voltages of AMR sensor were recorded depending on the time. The results of the real-time measurements are given in Fig. 5c. The electrical output voltage of the sensor based on the WB structure periodically changed and was observed to be stable over time. The real-time measurements of the AMR sensors show that the memory states of the sensor are hysteretic because they completely return to their initial state even in various H_{ext} with the positive and negative polarities. However, there is a fluctuation in the output voltages in the presence of a 20-Oe magnetic field, as shown in Fig. 5c. The reason for that magnitude of the external magnetic field values of 20 Oe and lower is not large enough to completely saturate the Py layer. The fluctuations are also compatible with AMR output voltage for $H = 20$ Oe in Fig. 5a.

In addition to the behavior of the angle-dependent electrical output signal and stability measurements, the sensitivities of both samples were calculated. Here, the sensitivity is equal to the first derivative of the R with respect to H_{ext} divided by the actual resistance value [28]. The sensitivity formula can be expressed as in Eq. (2).

$$S(H_{\text{ext}}) = [(dR(H_{\text{ext}})/dH_{\text{ext}})]/R(H_{\text{ext}}) \quad (2)$$

where S is sensitivity of the sample and R is resistance of the sample.

Figure 6a presents the sensitivity graph for the reference sample. According to Eq. (2), the sensitivity of the reference

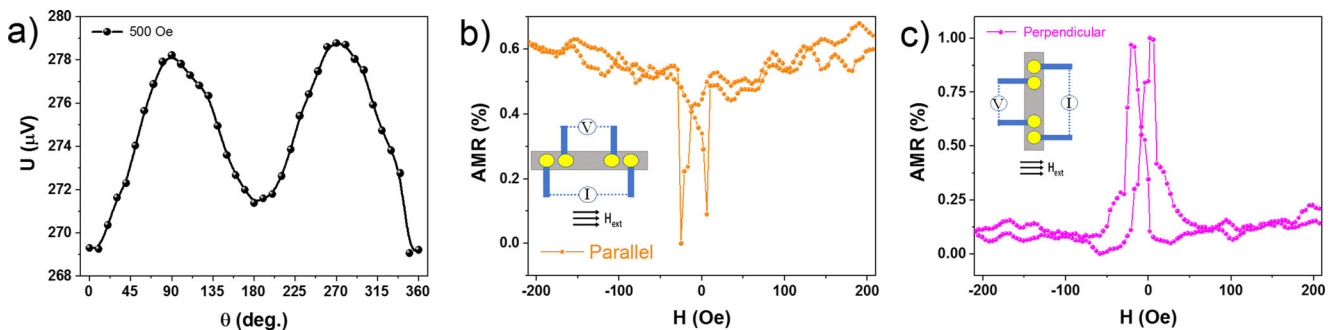


Fig. 4 Magnetoresistance characterizations of the AMR sensor with WB. **a** Angle-dependent U ratio of the sensor with WB under an external magnetic field of 500 Oe. **b** AMR ratio of AMR sensor with WB when M and J are parallel. **c** AMR ratio of AMR sensor with WB when M and J are perpendicular

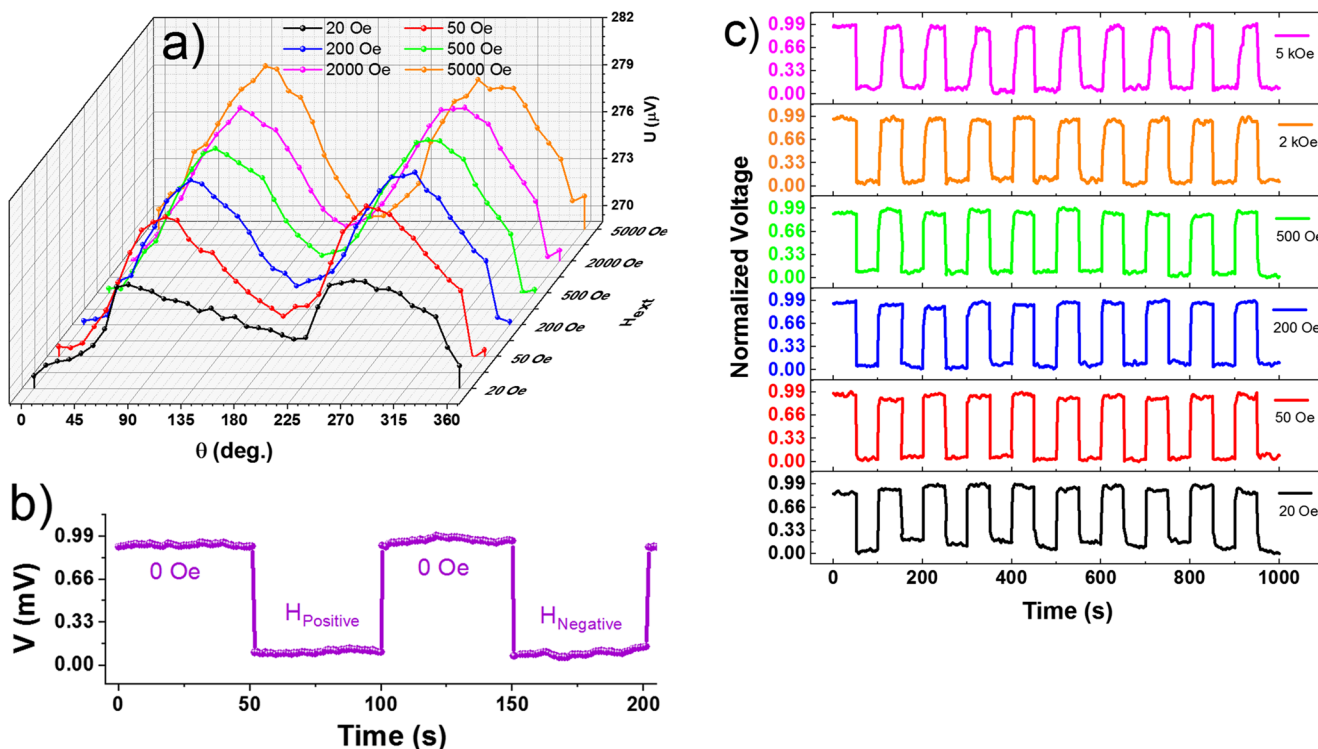


Fig. 5 **a** The angle-dependent electrical output voltage under the constant magnetic field for the Wheatstone bridge with barber pole. **b** The technique of the stability measurement under the magnetic field with

the positive and negative polarities for the AMR sensor based on WB structure. **c** Real-time measurements of the AMR sensor in various external magnetic fields with positive and negative polarities

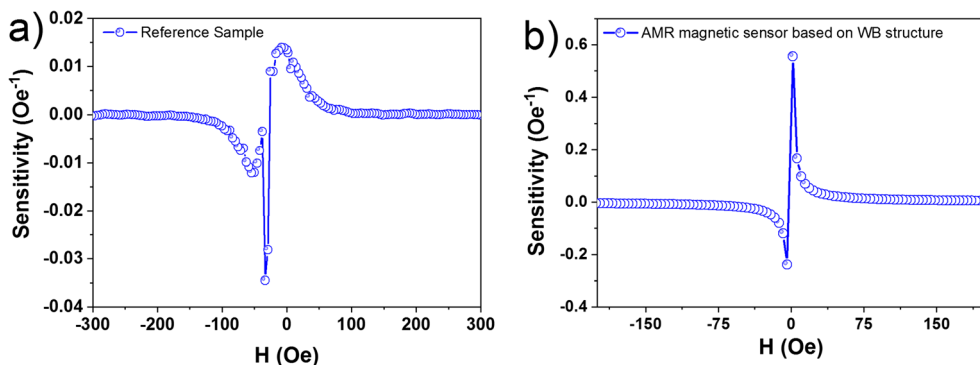
sample was calculated as 0.035 Oe^{-1} . When the sensor with the WB structure was used instead of the Hall bar structure, it was observed that sensitivity reaches a remarkable value. Figure 6b shows the sensitivity graph for the AMR sensor with WB and the sensitivity of the sensor was calculated as 0.55 Oe^{-1} . It can be deduced from the sensitivity comparison that WB structure provides more sensitivity as against Hall bar since sensitivity was increased almost 15 times when sensors with the WB structures were used instead of Hall bar structures.

magnetic and electrical properties have been studied in detail. First, both sensor structures exhibited uniaxial magnetic anisotropy, but it was observed that the periodically anisotropic behavior of the AMR sensor based on WB structure shifted 90° from the anisotropic behavior of the reference sample. This is because whether the applied H_{ext} and J are parallel or anti-parallel. Second, the angle-dependent electrical output voltage under the constant magnetic field for AMR sensors based on WB structure is compatible with $\cos^2\theta$ behavior from 50 up to 5000 Oe. However, for $H = 20 \text{ Oe}$, it was observed that there was a deviation from the theoretically predicted behavior. This means that the magnetic moments of the Py layer cannot fully be saturated by the H_{ext} . Third, in magnetotransport measurements, comparisons in terms of AMR ratio and sensitivity showed that (i) AMR ratio of the

4 Conclusion

In summary, two different AMR sensors based on conventional Hall bar and WB structures have been fabricated and their

Fig. 6 The sensitivity of the **a** AMR sensor and **b** reference sample. The sensitivity of the samples was calculated according to the sensitivity formula



WB structure is three times higher than the Hall bar reference sample and (ii) AMR sensor based on WB structure is almost 15 times more sensitive than the reference sample. This is proof that it achieved higher output voltage and a more sensitive sensor owing to the WB structure. Finally, the stability of the AMR sensor was tested in various H_{ext} with positive and negative polarities. The real-time measurements of the AMR sensors showed that the memory states of the sensor were hysteretic because they completely return to their initial state with versatile H_{ext} with the positive and negative polarities. Also, the response of the AMR sensor based on WB structure is quite stable even at various H_{ext} up to 5000 Oe.

Funding information This work was supported by the research fund of Gebze Technical University through project number 2018 A-105-44.

References

- Pannetier-Lecoecur, M., Parkkonen, L., Sergeeva-Chollet, N., Polovy, H., Fermon, C., Fowley, C.: Magnetocardiography with sensors based on giant magnetoresistance. *Appl. Phys. Lett.* **98**(15), 153705 (2011). <https://doi.org/10.1063/1.3575591>
- Ennen, I., Kappe, D., Rempel, T., Glenske, C., Hütten, A.: Giant magnetoresistance: basic concepts, microstructure, magnetic interactions and applications. *Sensors (Basel)*. **16**(6), 904 (2016). <https://doi.org/10.3390/s16060904>
- Hauser, M., Kraus, L., Ripka, P.: Giant magnetoimpedance sensors. *IEEE Instrum. Meas. Mag.* **4**(2), 28–32 (2001). <https://doi.org/10.1109/5289.930983>
- Zhukov, A., Ipatov, M., Zhukova, V.: Chapter 2 - advances in giant magnetoimpedance of materials. In: Buschow, K.H.J. (ed.) *Handbook of magnetic materials*, vol. 24, pp. 139–236. Elsevier (2015)
- Gider, S., Runge, B.U., Marley, A.C., Parkin, S.S.P.: The magnetic stability of spin-dependent tunneling devices. *Science*. **281**(5378), 797 (1998). <https://doi.org/10.1126/science.281.5378.797>
- Lee, W., Joo, S., Kim, S.U., Rhie, K., Hong, J., Shin, K.-H., Kim, K.H.: Magnetic bead counter using a micro-Hall sensor for biological applications. *Appl. Phys. Lett.* **94**(15), 153903 (2009). <https://doi.org/10.1063/1.3122142>
- Tumanski, S.: A new type of thin film magnetoresistive magnetometer—an analysis of circuit principles. *IEEE Trans. Magn.* **20**(5), 1720–1722 (1984). <https://doi.org/10.1109/TMAG.1984.1063221>
- Tumański, S., Stabrowski, M.: The optimization and design of magnetoresistive barber-pole sensors. *Sensors Actuators*. **7**(4), 285–295 (1985). [https://doi.org/10.1016/0250-6874\(85\)80008-1](https://doi.org/10.1016/0250-6874(85)80008-1)
- Kuijk, K., Gestel, W.V., Gorter, F.: The barber pole, a linear magnetoresistive head. *IEEE Trans. Magn.* **11**(5), 1215–1217 (1975). <https://doi.org/10.1109/TMAG.1975.1058886>
- Wang, C., Su, W., Hu, Z., Pu, J., Guan, M., Peng, B., Li, L., Ren, W., Zhou, Z., Jiang, Z., Liu, M.: Highly sensitive magnetic sensor based on anisotropic magnetoresistance effect. *IEEE Trans. Magn.* **54**(11), 1–3 (2018). <https://doi.org/10.1109/TMAG.2018.2846758>
- Sreevidya, P.V., Khan, J., Barshilia, H.C., Ananda, C.M., Chowdhury, P.: Development of two axes magnetometer for navigation applications. *J. Magn. Magn. Mater.* **448**, 298–302 (2018). <https://doi.org/10.1016/j.jmmm.2017.08.064>
- Bedoya-Pinto, A., Donolato, M., Gobbi, M., Hueso, L.E., Vavassori, P.: Flexible spintronic devices on Kapton. *Appl. Phys. Lett.* **104**(6), 062412 (2014). <https://doi.org/10.1063/1.4865201>
- Wang, Z., Wang, X., Li, M., Gao, Y., Hu, Z., Nan, T., Liang, X., Chen, H., Yang, J., Cash, S., Sun, N.-X.: Highly sensitive flexible magnetic sensor based on anisotropic magnetoresistance effect. *Adv. Mater.* **28**(42), 9370–9377 (2016). <https://doi.org/10.1002/adma.201602910>
- Brown, P., Beek, T., Carr, C., O'Brien, H., Cupido, E., Oddy, T., Horbury, T.S.: Magnetoresistive magnetometer for space science applications. *Meas. Sci. Technol.* **23**(2), 025902 (2012)
- McGuire, T., Potter, R.: Anisotropic magnetoresistance in ferromagnetic 3d alloys. *IEEE Trans. Magn.* **11**(4), 1018–1038 (1975). <https://doi.org/10.1109/TMAG.1975.1058782>
- Zhang, S.S.L., Vignale, G., Zhang, S.: Anisotropic magnetoresistance driven by surface spin-orbit scattering. *Phys. Rev. B*. **92**(2), 024412 (2015). <https://doi.org/10.1103/PhysRevB.92.024412>
- Ebert, H., Vernes, A., Banhart, J.: Magnetoresistance, anisotropic. In: Buschow, K.H.J., Cahn, R.W., Flemings, M.C., Ileschner, B., Kramer, E.J., Mahajan, S., Veysière, P. (eds.) *Encyclopedia of materials: science and technology*, pp. 5079–5083. Elsevier, Oxford (2001)
- Nazarov, A.V., da Silva, F.C.S., Pappas, D.P.: Arrays of magnetoresistive sensors for nondestructive testing. *J. Vac. Sci. Technol. A*. **22**(4), 1375–1378 (2004). <https://doi.org/10.1116/1.1743087>
- Popovic, R.S., Flanagan, J.A., Besse, P.A.: The future of magnetic sensors. *Sensors Actuators A Phys.* **56**(1), 39–55 (1996). [https://doi.org/10.1016/0924-4247\(96\)01285-X](https://doi.org/10.1016/0924-4247(96)01285-X)
- Vopalensky, M., Platil, A.: Temperature drift of offset and sensitivity in full-bridge magnetoresistive sensors. *IEEE Trans. Magn.* **49**(1), 136–139 (2013). <https://doi.org/10.1109/TMAG.2012.2220535>
- Dibbern, U.: Magnetic field sensors using the magnetoresistive effect. *Sensors Actuators*. **10**(1), 127–140 (1986). [https://doi.org/10.1016/0250-6874\(86\)80038-5](https://doi.org/10.1016/0250-6874(86)80038-5)
- Kocaman, B., Akdoğan, N.: Reduction of shunt current in buffer-free IrMn based spin-valve structures. *J. Magn. Magn. Mater.* **456**, 17–21 (2018). <https://doi.org/10.1016/j.jmmm.2018.02.008>
- Knorr, T.G., Hoffman, R.W.: Dependence of geometric magnetic anisotropy in thin iron films. *Phys. Rev.* **113**(4), 1039–1046 (1959). <https://doi.org/10.1103/PhysRev.113.1039>
- Thompson, S.M.: Magnetoresistive heads: physical phenomena. In: Buschow, K.H.J., Cahn, R.W., Flemings, M.C., Ileschner, B., Kramer, E.J., Mahajan, S., Veysière, P. (eds.) *Encyclopedia of materials: science and technology*, pp. 5095–5101. Elsevier, Oxford (2001)
- Dogra, A., Chowdhury, P., Ghosh, S.K., Gupta, S.K., Ravikumar, G.: Planar Hall effect in electrodeposited CoCu/Cu multilayer. *Appl. Phys. A*. **111**(1), 323–328 (2013). <https://doi.org/10.1007/s00339-013-7545-2>
- Bason, Y., Klein, L., Yau, J.-B., Hong, X., Ahn, C.H.: Giant planar Hall effect in colossal magnetoresistive La_{0.84}Sr_{0.16}MnO₃ thin films. *Appl. Phys. Lett.* **84**(14), 2593–2595 (2004). <https://doi.org/10.1063/1.1695197>
- Adeyeye, A.O., Win, M.T., Tan, T.A., Chong, G.S., Ng, V., Low, T.S.: Planar Hall effect and magnetoresistance in Co/Cu multilayer films. *Sensors Actuators A Phys.* **116**(1), 95–102 (2004). <https://doi.org/10.1016/j.sna.2004.03.042>
- Kubinski, D.J., Holloway, H.: Giant magnetoresistance in Co/Cu multilayers: influence of Co thickness at the first antiferromagnetic maximum. *J. Appl. Phys.* **79**(9), 7395–7397 (1996). <https://doi.org/10.1063/1.362449>

Publisher's note Springer Nature remains neutral with regard to jurisdictional claims in published maps and institutional affiliations.